



**HAL**  
open science

# IMPROVING THE NEAR-FIELD ACOUSTICAL HOLOGRAPHY RESULTS BY USING THE REGRESSIVE DISCRETE FOURIER SERIES

Alexander Pasqual

► **To cite this version:**

Alexander Pasqual. IMPROVING THE NEAR-FIELD ACOUSTICAL HOLOGRAPHY RESULTS BY USING THE REGRESSIVE DISCRETE FOURIER SERIES. ICSV20 - 20th International Congress on Sound and Vibration, Jul 2013, Bangkok, Thailand. p.1-8. hal-00846063

**HAL Id: hal-00846063**

**<https://hal.science/hal-00846063>**

Submitted on 18 Jul 2013

**HAL** is a multi-disciplinary open access archive for the deposit and dissemination of scientific research documents, whether they are published or not. The documents may come from teaching and research institutions in France or abroad, or from public or private research centers.

L'archive ouverte pluridisciplinaire **HAL**, est destinée au dépôt et à la diffusion de documents scientifiques de niveau recherche, publiés ou non, émanant des établissements d'enseignement et de recherche français ou étrangers, des laboratoires publics ou privés.

# IMPROVING THE NEAR-FIELD ACOUSTICAL HOLOGRAPHY RESULTS BY USING THE REGRESSIVE DISCRETE FOURIER SERIES

Alexander Mattioli Pasqual

*Federal University of Minas Gerais, Department of Mechanical Engineering, 31270-901, Belo Horizonte/MG, Brazil*

*e-mail: [ampasqual@demec.ufmg.br](mailto:ampasqual@demec.ufmg.br)*

The planar Near-field Acoustical Holography (NAH) is a non-contact technique that can be used to estimate the vibration pattern of a planar body from the sound pressure it produces on a planar microphone array. The conventional NAH relies on the spatial Discrete Fourier Transform (DFT), requiring the microphone array to be larger than the source to reduce the spatial windowing effects due to the finite measurement aperture. This constraint can be overcome by “patch” NAH procedures, such as the Statistically Optimal NAH (SONAH). However, the patch algorithms are less efficient and differ significantly from the conventional NAH algorithm. As an alternative, this work proposes an improved Fourier-based NAH technique, which replaces the DFT by the Regressive Discrete Fourier Series (RDFS). Unlike the former, the latter lets the period of the Fourier series be larger than the measurement aperture, and the number of wavenumber components be smaller than the number of microphones. Then, the Fourier coefficients are obtained in the least-squares sense. Thus, by setting the period and the number of spectrum lines, a microphone array significantly smaller than the source can be used, which is shown in this paper through numerical simulations. Finally, the computation time and the algorithm structure of the DFT and RDFS-based NAH are similar; the only difference being the way the space-wavenumber transformation is done.

## 1. Introduction

Near-field Acoustical Holography (NAH) is a powerful technique to reconstruct 3-D sound fields from 2-D acoustical data, especially in inverse source reconstruction. Maynard *et al*<sup>1</sup> introduced the NAH in the 1980s, and the holographic procedure they proposed, based on the Discrete Fourier Transform (DFT), is still widely used and will be referred here as “conventional” NAH, or DFT-based NAH. Because an efficient algorithm is available to compute the DFT, the Fast Fourier Transform (FFT), the conventional NAH is a very fast procedure for sound field reconstruction.

The conventional NAH can be used in planar, cylindrical and spherical coordinates.<sup>2</sup> In planar NAH, a planar microphone array is used to sample the sound field, and the reconstruction procedure is based on the direct and inverse 2-D DFT, as well as on a wave propagation model. In order to provide accurate results, three issues must be considered: spatial aliasing, ill-posedness of the inverse reconstruction problem, and finite measurement aperture. The first issue can be overcome by

using a large enough number of microphones. For the second, a regularization technique must be used to prevent unstable solutions.<sup>3</sup> The third issue can be dealt with by making the microphone array larger than the sound source extension, otherwise spatial windowing effects will degrade the holographic results.<sup>2</sup> This work focuses on the finite measurement aperture issue.

As far as large sources are concerned, a microphone array covering all the source area is not practical. If a smaller array is used in conventional NAH, the DFT will lead to wrap-around errors due to the spatial windowing that will degrade the holography results. The search for smaller arrays has led to the “patch” NAH procedures, such as the Statistically Optimal NAH (SONAH)<sup>4</sup>, which is not based on the Fourier transform. However, the patch NAH algorithms usually require more computation time and differ significantly from the well established DFT-based NAH algorithm.

As an alternative to SONAH, this work proposes an improved Fourier-based NAH technique to reduce the spatial windowing effects in planar NAH. In order to address this issue, the Regressive Discrete Fourier Series (RDFS) proposed by Arruda<sup>5</sup> is used instead of the DFT. It is shown through numerical simulations of 1-D and 2-D extended sources that a microphone array significantly smaller than the source size can be used with the improved method. Finally, the computation time and the algorithm structure of the DFT and RDFS-based NAH are similar; the only difference being the way the space-wavenumber transformation is done.

## 2. The regressive discrete Fourier series

Consider a continuous deterministic signal in the space and wavenumber domains. It is known that sampling in one domain leads to a periodized version of the signal in the other domain. Thus, for Fourier analysis purposes, finite length signals to be processed in a digital computer can be considered as periodic signals. Besides, most of the periodic signals can be satisfactorily represented by its Fourier series, with the corresponding coefficients being determined from integration over one full period of the signal. However, if this period is given, it is possible to estimate the Fourier coefficients from data known in a portion of the signal period. In this case, a number of samples in the space domain larger than the number of wavenumber lines can be taken, so that a least-squares fit leads to an approximation of the desired coefficients. This is the basic idea of the RDFS.

The RDFS differs from the DFT by the fact that the latter makes the period equal to the data block length, whereas the former allows these values to be different. In addition, unlike the RDFS, the DFT requires equally spaced data and uses the same number of samples in the space and wavenumber domains. In the following, an overview of the one- and two-dimensional RDFS for equally spaced data is presented. For non-equally spaced data, the reader is referred to Arruda<sup>6</sup>.

### 2.1 One-dimensional RDFS

The direct and inverse Fourier transforms of a continuous function  $f(x)$  are given by<sup>2</sup>

$$F(k_x) = \int_{-\infty}^{\infty} f(x) e^{-jk_x x} dx, \quad f(x) = \frac{1}{2\pi} \int_{-\infty}^{\infty} F(k_x) e^{jk_x x} dk_x, \quad (1)$$

where  $j = \sqrt{-1}$ ,  $x$  is the position, and  $k_x$  is the wavenumber. Now, consider  $N$  and  $M$  equally spaced samples of  $f(x)$  and  $F(k_x)$ , respectively, so that  $f_n \equiv f(n\Delta x)$  and  $F_m \equiv F(m\Delta k_x)$ , where  $-N/2 \leq n < N/2$  and  $-M/2 \leq m < M/2$  are integers. Then, these expressions can be approximated by

$$F_m \approx \Delta x \sum_{n=-N/2}^{N/2-1} f_n e^{-j2\pi mn\Delta x/L}, \quad f_n \approx \frac{1}{L} \sum_{m=-M/2}^{M/2-1} F_m e^{j2\pi mn\Delta x/L}, \quad (2)$$

where  $L$  is the period of the Fourier series (notice that  $\Delta k_x = 2\pi/L$ ).

Let  $\mathbf{f}$  and  $\mathbf{F}$  be column vectors containing the values  $f_n$  and  $F_m$ . The approximation for the inverse Fourier transform can then be written in matrix notation as

$$\mathbf{f} \approx \mathbf{W}\mathbf{F}, \quad (3)$$

where  $\mathbf{W}$  is an  $N \times M$  matrix whose entries are

$$W_{nm} = \frac{1}{L} e^{j2\pi mn\Delta x / L}. \quad (4)$$

If  $N > M$ , Eq. (3) becomes an overdetermined linear system, and thus the least-squares method leads to the following optimal approximation for the Fourier coefficients:

$$\mathbf{F}^{\text{opt}} = (\mathbf{W}^H \mathbf{W})^{-1} \mathbf{W}^H \mathbf{f}, \quad (5)$$

where the superscript H indicates the complex conjugate transpose. Finally, the corresponding approximation for the inverse Fourier transform is

$$\mathbf{f}^{\text{opt}} = \mathbf{W}\mathbf{F}^{\text{opt}}. \quad (6)$$

This least-squares solution is the RDFS, which can be used to reduce the spatial windowing effects by letting the period be larger than the data length, i.e.,  $L > N\Delta x$ . Usually, the choice of  $L$  and  $M$  is based on the prior knowledge about the signal, although an optimization procedure could be used to obtain  $L$  for a given  $M$ .<sup>6</sup> These two values play a major role in the conditioning of the problem. As a general guideline,  $L$  must be made smaller as  $M$  increases in order to avoid ill-conditioned matrices. In the limit,  $M = N$  and  $L = N\Delta x$ ; in addition, if a change of the indices  $m$  and  $n$  is done, inspection of Eq. (2) reveals that the RDFS becomes the DFT.

## 2.2 Two-dimensional RDFS

This section extends the developments of Section 2.1 to 2-D signals defined in the  $xy$  plane. Therefore, in the following, the same approach is adopted to derive the equations for the 2-D RDFS. The direct and inverse 2-D Fourier transforms of a continuous function  $f(x,y)$  are<sup>2</sup>

$$F(k_x, k_y) = \int_{-\infty}^{\infty} \int_{-\infty}^{\infty} f(x, y) e^{-j(k_x x + k_y y)} dx dy, \quad f(x, y) = \frac{1}{4\pi^2} \int_{-\infty}^{\infty} \int_{-\infty}^{\infty} F(k_x, k_y) e^{j(k_x x + k_y y)} dk_x dk_y, \quad (7)$$

where  $k_x$  and  $k_y$  are the wavenumbers in the  $x$  and  $y$  directions. Now, let  $f_{n_x, n_y} \equiv f(n_x \Delta x, n_y \Delta y)$  be samples of  $f(x, y)$  uniformly distributed over a rectangular grid, where  $-N_x/2 \leq n_x < N_x/2$  and  $-N_y/2 \leq n_y < N_y/2$  are integers. Similarly,  $F_{m_x, m_y} \equiv F(m_x \Delta k_x, m_y \Delta k_y)$  are samples of  $F(k_x, k_y)$  with  $-M_x/2 \leq m_x < M_x/2$  and  $-M_y/2 \leq m_y < M_y/2$ . Then, the inverse transform can be approximated by

$$f_{n_x, n_y} \approx \frac{1}{L_x L_y} \sum_{m_x=-M_x/2}^{M_x/2-1} \sum_{m_y=-M_y/2}^{M_y/2-1} F_{m_x, m_y} e^{j2\pi(m_x n_x \Delta x / L_x + m_y n_y \Delta y / L_y)}, \quad (8)$$

where  $L_x$  and  $L_y$  are the periods of the Fourier series in the  $x$  and  $y$  directions (notice that  $\Delta k_x = 2\pi/L_x$  and  $\Delta k_y = 2\pi/L_y$ ).

Let  $\mathbf{f}$  and  $\mathbf{F}$  be  $N_x \times N_y$  and  $M_x \times M_y$  matrices, containing the values  $f_{n_x, n_y}$  and  $F_{m_x, m_y}$ , respectively. Equation (8) can then be written in matrix notation as

$$\mathbf{f} \approx \mathbf{W}^{(x)} \mathbf{F} \mathbf{W}^{(y)}, \quad (9)$$

where  $\mathbf{W}^{(x)}$  and  $\mathbf{W}^{(y)}$  are  $N_x \times M_x$  and  $M_y \times N_y$  matrices. By letting  $\xi = x, y$ , these matrices are

$$W_{n_\xi m_\xi}^{(\xi)} = \frac{1}{L_\xi} e^{j2\pi n_\xi m_\xi \Delta \xi / L_\xi}. \quad (10)$$

If  $N_x > M_x$  and  $N_y > M_y$ , the least-squares method leads to the following optimal approximation for the Fourier coefficients:

$$\mathbf{F}^{\text{opt}} = [(\mathbf{W}^{(x)})^H \mathbf{W}^{(x)}]^{-1} (\mathbf{W}^{(x)})^H \mathbf{f} (\mathbf{W}^{(y)})^H [\mathbf{W}^{(y)} (\mathbf{W}^{(y)})^H]^{-1}. \quad (11)$$

Finally, the corresponding approximation for the inverse two-dimensional Fourier transform is

$$\mathbf{f}^{\text{opt}} = \mathbf{W}^{(x)} \mathbf{F}^{\text{opt}} \mathbf{W}^{(y)}. \quad (12)$$

This least-squares solution is the two-dimensional version of the RDFS developed in Section 2.1. Hence, the discussion presented at the end of that section remains valid.

### 3. The RDFS-based NAH

Planar NAH is a useful tool to investigate the sound radiation from planar sources (or nearly planar), such as vibrating plates. Figure 1 illustrates a typical geometric configuration for planar NAH. The sources are placed on an infinite plane called “source plane”, defined by  $z = z_s$ . As a matter of fact, it is not required that the sources be located at this plane, but they must be confined to  $z \leq z_s$ , as well as all the scattering objects. Therefore, the conditions for a half-space problem are fulfilled. Then, by using a wave propagation model, the 3-D sound field in the half-space  $z \geq z_s$  can be estimated from 2-D acoustic data (usually sound pressure), which are obtained on an infinite plane parallel to the source plane. This plane, defined by  $z = z_h$ , is called “measurement plane”, and the resulting data are called “hologram”. In addition, the measurement plane must be very close to the source plane if we are interested in obtaining a detailed reconstruction of the acoustic field on  $z = z_s$ .

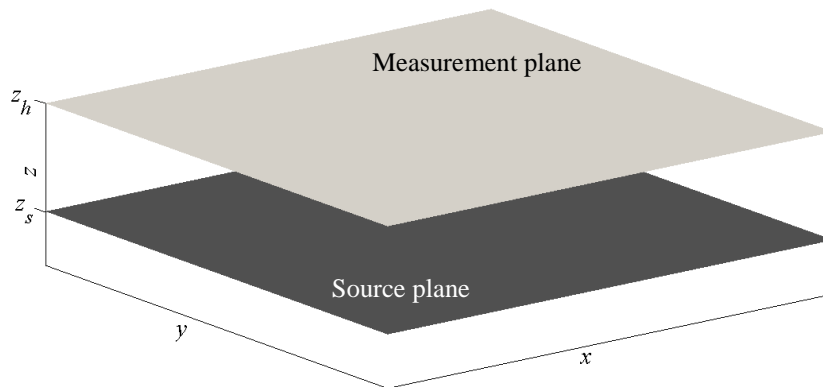


**Figure 1.** Measurement plane ( $z = z_h$ ) and source plane ( $z = z_s$ ) in planar NAH.

Due to the great computational speed, Fourier analysis and synthesis has been applied in planar NAH since its beginnings. Basically, the steps involved in Fourier-based NAH are:

1. Measurement of the sound pressure field on a given plane;
2. Transformation of the measured field to the wavenumber domain;
3. Computation of the acoustic field on the reconstruction plane in the wavenumber domain;
4. Transformation of the computed acoustic field to the space domain.

Step 1 is accomplished by using a planar microphone array placed on the measurement plane. Since it must be of finite length and only a finite number of transducers can be used, errors due to windowing effects and spatial aliasing may arise. Let  $p(x, y, z)$  be the pressure field, and  $p_{n_x, n_y}(z) \equiv p(n_x \Delta x, n_y \Delta y, z)$  be samples uniformly distributed over a rectangular grid, where  $n_x$  and  $n_y$  are the same integers defined in Section 2.2. Thus, a planar array of  $N_x N_y$  equally spaced microphones leads to the values  $p_{n_x, n_y}(z_h) \equiv p(n_x \Delta x, n_y \Delta y, z_h)$ , where  $\Delta x$  and  $\Delta y$  are the distances between them in the  $x$  and  $y$  directions. These values can be arranged in an  $N_x \times N_y$  matrix,  $\mathbf{p}_h$ .

In conventional NAH, the direct and inverse DFT are used in steps 2 and 4, respectively. In this work, we propose to use the RDFS described in Section 2 to undertake these tasks. Let

$P(k_x, k_y, z_h)$  be the 2-D Fourier transform of  $p(x, y, z_h)$ , so that the replacement of  $\mathbf{f}$  by  $\mathbf{p}_h$  in Eq. (11) yields the optimal approximation for the Fourier coefficients of the measured field:

$$\mathbf{P}_h^{\text{opt}} = [(\mathbf{W}^{(x)})^H \mathbf{W}^{(x)}]^{-1} (\mathbf{W}^{(x)})^H \mathbf{p}_h (\mathbf{W}^{(y)})^H [\mathbf{W}^{(y)} (\mathbf{W}^{(y)})^H]^{-1}. \quad (13)$$

In step 3, a propagation model in the wavenumber domain is applied. As far as linear sound wave propagation in a half-space is concerned, it can be shown that<sup>2</sup>

$$P(k_x, k_y, z_r) = P(k_x, k_y, z_h) e^{jk_z(z_r - z_h)}, \quad z_r \geq z_s, \quad (14)$$

where  $P(k_x, k_y, z_r)$  is the 2-D Fourier transform of  $p(x, y, z_r)$ ,  $z_r$  is the position of the reconstruction plane,  $k_z^2 = k^2 - k_x^2 - k_y^2$ ,  $k = 2\pi f/c$  is the acoustic wavenumber,  $f$  is the frequency, and  $c$  is the sound speed. In addition, the 2-D transform of the normal surface velocity on the reconstruction plane is<sup>2</sup>

$$V(k_x, k_y, z_r) = \frac{k_z}{\rho c k} P(k_x, k_y, z_h) e^{jk_z(z_r - z_h)}, \quad z_r \geq z_s, \quad (15)$$

where  $\rho$  is the medium density. Substitution of  $P(k_x, k_y, z_h)$  by the entries of  $\mathbf{P}_h^{\text{opt}}$  in Eqs. (14) and (15) leads to an estimation of the 2-D Fourier transform of the sound pressure,  $\mathbf{P}_r^{\text{opt}}$ , and the normal velocity,  $\mathbf{V}_r^{\text{opt}}$ , on the reconstruction plane. Finally, the reconstructed pressure and velocity fields are obtained by letting  $\mathbf{P}_r^{\text{opt}} = \mathbf{F}^{\text{opt}}$  and  $\mathbf{V}_r^{\text{opt}} = \mathbf{F}^{\text{opt}}$  in Eq. (12), respectively. For the latter, one has

$$\mathbf{v}_r^{\text{opt}} = \mathbf{W}^{(x)} \mathbf{V}_r^{\text{opt}} \mathbf{W}^{(y)}. \quad (16)$$

Note that if the reconstruction plane is located at  $z_r > z_h$ , one has a forward propagation problem, which poses no difficulties because the sound field tends to smooth as  $z$  increases. On the other hand, if the reconstruction plane is somewhere between the measurement and source planes ( $z_s \leq z_r < z_h$ ), we must deal with an inverse propagation problem, which is usually ill-conditioned because the hologram is not sensitive to all the sound field details on the reconstruction plane. Thus, small measurement errors in the hologram might be greatly amplified by the inverse propagator due to the presence of strongly decaying waves, which correspond to high-wavenumber components ( $k_x^2 + k_y^2 > k^2 \Rightarrow k_z = j|k_z|$ ). This issue can be addressed by a regularization method, e.g., a low-pass filter can be applied between steps 2 and 3 described above.<sup>2</sup> In this work, the hologram is assumed error free, so that the ill-conditioning associated to the inverse propagation is of minor interest.

## 4. Simulation results

This section gives simulation results in order to show the advantages of the RDFS over the DFT in NAH. The normal velocity on the source plane is reconstructed from pressure data on the measurement plane. Here, the “measured” pressure is calculated by solving the forward propagation problem as follows: a simple velocity pattern on the source plane is chosen, so that a closed-form expression for  $V(k_x, k_y, z_s)$  is obtained. Then, substitution of  $V(k_x, k_y, z_s)$  in Eq. (15) leads to  $P(k_x, k_y, z_h)$ . Finally, by letting  $P(k_x, k_y, z_h) = F(k_x, k_y)$  and  $(x, y)$  be the microphone positions on the right of Eq. (7), the “measured” pressure is obtained. In order to produce an accurate hologram for the simulations, Eq. (7) is approximated by a rectangular integration rule covering a large densely sampled area in the  $k_x k_y$  plane. Besides, it is assumed that  $c = 343$  m/s and  $\rho = 1.21$  kg/m<sup>3</sup>.

### 4.1 One-dimensional extended source

This first example is an extended source whose vibration pattern is a function of  $x$ , but remains constant in the  $y$  direction. Thus, it is an infinite radiator in  $y$  with  $k_y = 0$ . The “exact” normal velocity on the source plane is chosen to be

$$v(x, z_s) = \cos(k_{x0}x)\Pi(x/L_s), \quad (17)$$

where  $L_s$  is the source length and  $\Pi(\cdot)$  is the rectangular function. In particular, we let  $k_{x0} = 7\pi/L_s$  and  $L_s = 2$  m. The “exact” curve in Fig. 2-c shows this signal.

The 1-D Fourier transform of  $v(x, z_s)$  is the convolution of the Fourier transforms of  $\cos(k_{x0}x)$  and  $\Pi(x/L_s)$ , which yields

$$V(k_x, z_s) = \frac{L_s}{2} \left\{ \text{sinc} \left[ \frac{(k_x - k_{x0})L_s}{2} \right] + \text{sinc} \left[ \frac{(k_x + k_{x0})L_s}{2} \right] \right\}, \quad (18)$$

where  $\text{sinc}(u) \equiv \sin(u)/u$ . Substitution of Eq. (18) into (15) with  $z_r = z_s$  leads to a closed-form expression for  $P(k_x, z_h)$ . The “analytical” curves in Fig. 2-d and 2-b show  $V(k_x, z_s)$  and  $P(k_x, z_h)$ , respectively. The latter is evaluated for  $f = 1$  kHz and  $z_h - z_s = 0.1$  m. Then, the hologram is obtained as described above, which is shown in Fig. 2-a, where the circles indicate the microphone positions. An array of  $N = 64$  microphones with  $\Delta x = 1/N$  is simulated, and thus the aperture is  $(N-1)\Delta x = 0.98$  m, i.e., nearly a half of the source length.

Now, the DFT- and RDFS-based NAH procedures are used to estimate  $v(x, z_s)$  from these 64 samples of  $p(x, y, z_h)$ , which are arranged in a column vector  $\mathbf{p}_h$ . The DFT of  $\mathbf{p}_h$  leads to the blue discrete spectrum shown in Fig. 2-b. For the RDFS, a period equals to the source length is used ( $L = L_s = 2$  m), and the number of samples in the wavenumber domain is chosen to be  $M = 32$ . Then, the vector containing the optimal Fourier coefficients,  $\mathbf{P}_h^{\text{opt}}$ , is obtained by letting  $\mathbf{f} = \mathbf{p}_h$  in Eq. (5), which is the red discrete spectrum shown in Fig. 2-b.

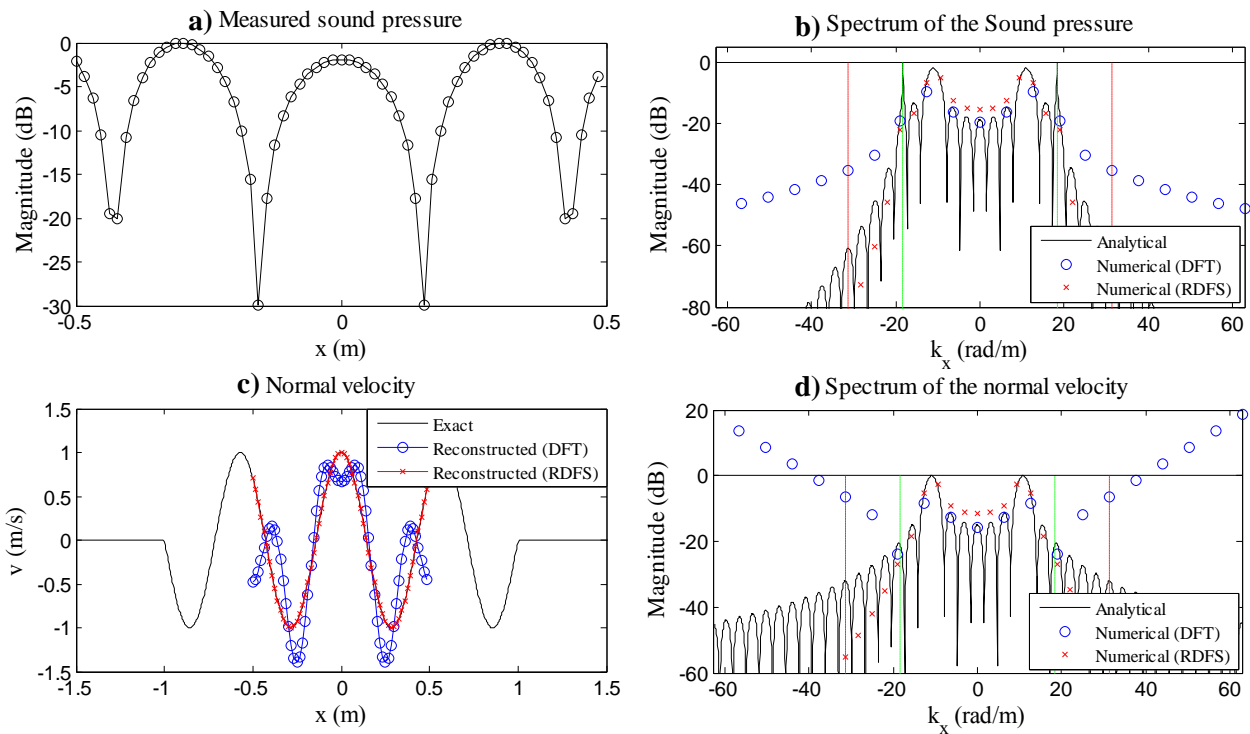


**Figure 2.** Simulation results for a 1-D extended source.

The period chosen for the RDFS is nearly twice the measurement aperture. Therefore, the wavenumber resolution is also nearly twice the resolution obtained by the DFT method, as Fig. 2-b reveals. Besides, the DFT leads to an accurate approximation of the pressure spectrum in the low-wavenumber range, but it overestimates the Fourier coefficients for high wavenumbers, which correspond to evanescent waves that have a minor contribution to the measured sound field. The vertical green lines in Figs. 2-b and 2-d indicate the acoustic wavenumber  $k$  (waves with  $|k_x| > k$  present a strongly decaying rate along the  $z$  direction). The inverse propagator, Eq. (15), greatly amplifies

these errors, as can be noticed in Fig. 2-d. In order to provide a stable solution, the signal is low-pass filtered (the vertical red lines indicate the cut-off of the chosen filter). Unlike the DFT, the error (in dB) in the pressure spectrum produced by the RDFS method tends to be more uniformly distributed over  $k_x$ , so that the propagator does not lead to error amplification (see Fig. 2-d). Thus, as far as this example is concerned, there is no need for low-pass filtering the signal.

Finally, Fig. 2-c shows that the RDFS method leads to an almost perfect source reconstruction, even for a small measurement aperture, whereas the DFT method does not provide good results and requires low-pass filtering to avoid unstable solutions.

## 4.2 Two-dimensional extended source

The next example is a 2-D planar source whose normal velocity is chosen to be

$$v(x, y, z_s) = \cos(k_{x0}x) \cos(k_{y0}y) \Pi(x/L_{sx}) \Pi(y/L_{sy}), \quad (19)$$

where  $L_{sx}$  and  $L_{sy}$  are the source lengths in the  $x$  and  $y$  directions. In the simulations, we use  $k_{x0} = 5\pi/L_{sx}$ ,  $k_{y0} = 3\pi/L_{sy}$ ,  $L_{sx} = 4$  m and  $L_{sy} = 2$  m. Similarly to the previous example, the following closed-form expression for the 2-D Fourier transform of  $v(x, y, z_s)$  can be obtained:

$$V(k_x, k_y, z_s) = \frac{L_{sx}L_{sy}}{4} \left\{ \text{sinc} \left[ \frac{(k_x - k_{x0})L_{sx}}{2} \right] + \text{sinc} \left[ \frac{(k_x + k_{x0})L_{sx}}{2} \right] \right\} \left\{ \text{sinc} \left[ \frac{(k_y - k_{y0})L_{sy}}{2} \right] + \text{sinc} \left[ \frac{(k_y + k_{y0})L_{sy}}{2} \right] \right\}. \quad (20)$$

Figure 3 shows  $v(x, y, z_s)$  on the left, and  $V(k_x, k_y, z_s)$  on the right.

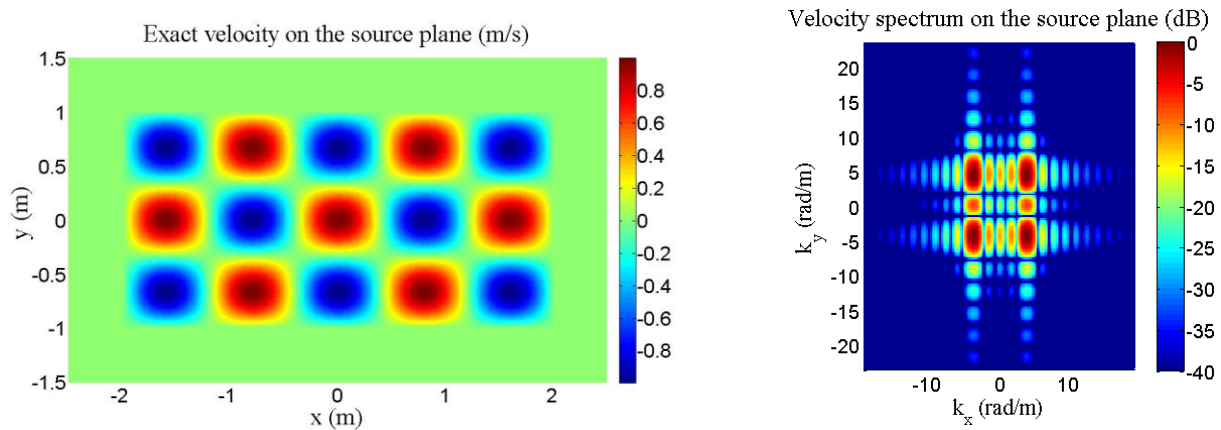


**Figure 3.** Two-dimensional planar source in the space (on the left) and wavenumber (on the right) domains.

Again, substitution of Eq. (20) into (15) leads to an expression for  $P(k_x, k_y, z_h)$ , which is evaluated for  $f = 1$  kHz and  $z_h - z_s = 0.1$  m. Then, the hologram is obtained in a similar fashion as for the 1-D example. This is shown in Fig. 4, where the black dots indicate the measurement points. A square grid made up of  $N_x = N_y = 32$  points in the  $x$  and  $y$  directions is used, with  $\Delta x = 0.8/N_x$  and  $\Delta y = 0.8/N_y$ . Therefore, the measurement aperture is a square of side  $(N_x - 1)\Delta x = 0.775$  m.

Now, the DFT- and RDFS-based NAH procedures are used to estimate  $v(x, y, z_s)$  from these  $32 \times 32 = 1024$  samples of  $p(x, y, z_h)$ , which are arranged in a square matrix  $\mathbf{p}_h$ . The 2-D FFT of  $\mathbf{p}_h$  leads to the discrete spectrum for the DFT method. For the RDFS, periods that match the source size are used, i.e.,  $L_x = L_{sx} = 4$  m and  $L_y = L_{sy} = 2$  m; and the numbers of samples in the  $k_x k_y$  plane is chosen to be  $M_x = M_y = 8$ . Then, Eq. (13) gives the optimal Fourier coefficients,  $\mathbf{P}_h^{\text{opt}}$ .

Next, in both methods, the inverse propagator is applied. As usual, the DFT-based NAH procedure requires low-pass filtering to provide a stable solution. Finally, application of the inverse two-dimensional DFT and Eq. (16) to the computed velocity spectrum leads to the reconstructed field by the DFT and RDFS methods, respectively. Figure 5 shows a comparison between the reconstruction results obtained by these methods with the exact velocity pattern. It can be noticed that the RDFS leads to a relevant improvement in source reconstruction by Fourier-based NAH.

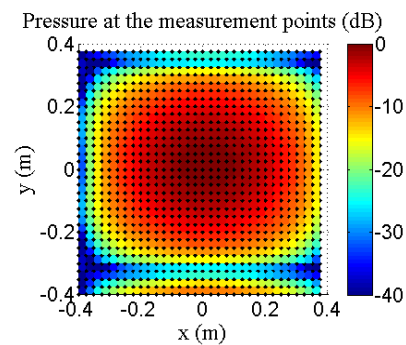


**Figure 4.** Simulated hologram in a square measurement grid with  $32 \times 32$  points.

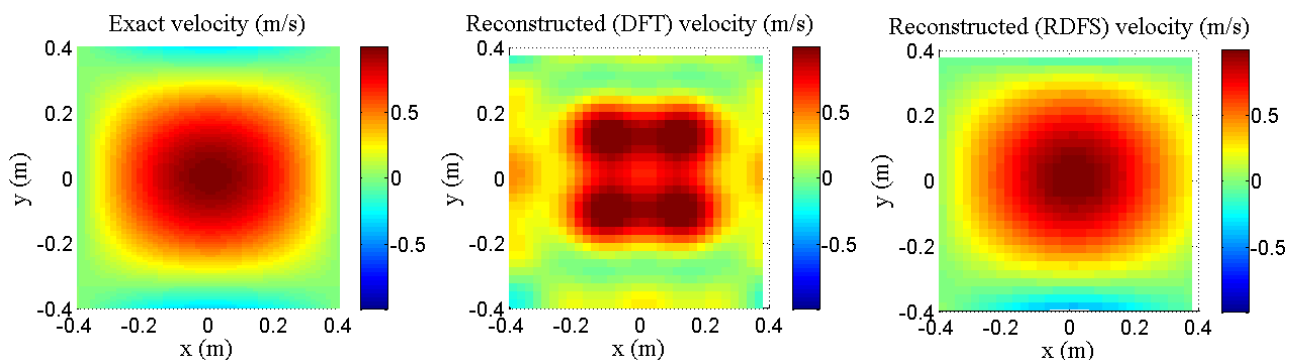


**Figure 5.** “Exact” and reconstructed velocity fields by the DFT and RDFS methods.

## 5. Conclusions

This work dealt with inverse source reconstruction by planar NAH with small measurement apertures. In order to reduce the spatial windowing effects that degrade the holography results in the conventional (DFT-based) NAH, a procedure based on the RDFS was used. It was shown through numerical examples that, unlike the DFT method, the RDFS leads to an excellent reconstructed velocity field, even for a measurement aperture significantly smaller than the source.

## Acknowledgments

The author wishes to acknowledge the financial support of the *Coordenação de Aperfeiçoamento de Pessoal de Nível Superior* (CAPES, Brazil), the *Conselho Nacional de Desenvolvimento Científico e Tecnológico* (CNPq, Brazil), and the *Programa Institucional de Auxílio à Pesquisa de Doutores Recém-Contratados da PRPq/UFMG* (Federal University of Minas Gerais, Brazil).

## REFERENCES

- <sup>1</sup> Maynard, J. D., Williams, E. G. and Lee, Y. Nearfield acoustic holography: I. Theory of generalized holography and the development of NAH, *The Journal of the Acoustical Society of America*, **78** (4), 1395–1413, (1985).
- <sup>2</sup> Williams, E. G. *Fourier Acoustics: Sound Radiation and Nearfield Acoustical Holography*, Academic Press, London, 15–114, (1999).
- <sup>3</sup> Williams, E. G. Regularization methods for near-field acoustical holography, *The Journal of the Acoustical Society of America*, **110** (4), 1976–1988, (2001).
- <sup>4</sup> Steiner, R. and Hald, J. Near-field acoustical holography without the errors and limitations caused by the use of spatial DFT, *International Journal of Acoustics and Vibration*, **6** (2), 83–89, (2001).
- <sup>5</sup> Arruda, J. R. F. Surface smoothing and partial spatial derivatives computation using a regressive discrete Fourier series, *Mechanical Systems and Signal Processing*, **6** (1), 41–50, (1992).
- <sup>6</sup> Arruda, J. R. F. Analysis of non-equally spaced data using a regressive discrete Fourier series, *Journal of Sound and Vibration*, **156** (3), 571–574, (1992).